COVER SHEET

Thermal decomposition of ammonium jarosite $(NH_4)Fe_3(SO_4)_2(OH)_6$

Ray L. Frost•, Rachael-Anne Wills, J. Theo Kloprogge, and Wayde Martens

Inorganic Materials Research Program, School of Physical and Chemical Sciences, Queensland University of Technology, GPO Box 2434, Brisbane Queensland 4001, Australia.

Abstract

Thermogravimetry combined with mass spectrometry has been used to study the thermal decomposition of a synthetic ammonium jarosite. Five mass loss steps are observed at 120, 260, 389, 510 and 541 °C. Mass spectrometry through evolved gases confirms these steps as loss of water, dehydroxylation, loss of ammonia and loss of sulphate in two steps. Changes in the molecular structure of the ammonium jarosite were followed by infrared emission spectroscopy (IES). This technique allows the infrared spectrum at the elevated temperatures to be obtained. IES confirms the dehydroxylation to have taken place by 300 °C and the ammonia loss by 450 °C. Loss of the sulphate is observed by changes in band position and intensity after 500 °C.

Keywords: ammonium jarosite, dehydroxylation, infrared emission spectroscopy, thermogravimetric analysis

Introduction

The jarosite mineral group has been extensively studied [1]. Jarosite was first discovered in 1852 in ravines in the mountainous coast of southeastern Spain. Ammonium jarosite $(NH_4)Fe_3(SO_4)_2(OH)_6$ was discovered in a black lignitic shale near Panguitch, Utah, USA [2]. The mineral has also been located in several other USA sites as well as in Germany, Austria and Venezuela [3]. The mineral has been associated with ammonium alum[3]. Interest in such minerals and their thermal stability rests with the possible identification of these minerals and dehydrated paragenetically related minerals on planets and on Mars. The existence of these minerals on planets would give a positive indication of the existence or at least pre-existence of water on Mars. Further such minerals are formed through crystallisation from solutions. Whether or not ammonium jarosite is found in such environments is unknown. One of the moons of Saturn, Cassini, has been reported to have an atmosphere of nitrogen/ammonia and hence a mineral such as ammonium jarosite could exist on this planet.

The formation of the mineral is rare since concentrated ammonium containing solutions are not common. The ammonium must come from the decomposition of organic substances or the biological activity associated with this organic matter. It has been shown that *Thiobacillus ferrooxidans* acts as a catalyst in the formation of

• Author to whom correspondence should be addressed (r.frost@qut.edu.au)

jarosite [4]. The importance of jarosite formation and its decomposition depends upon its presence in soils, sediments and evaporate deposits [5]. The presence of bacteria such as *Thiobacillus ferrooxidans* contribute to both jarosite and ammonium jarosite formation. These types of deposits have formed in acid soils where the pH is less than 3.0 [6]. Such acidification results from the oxidation of pyrite which may be from bacterial action or through air-oxidation or both.

The thermal decomposition of jarosites has been studied for considerable time [7-11]. Some studies of the thermal decomposition of ammonium jarosite have been undertaken [12, 13]. There have also been many studies on related minerals such as the Fe(II) and Fe(III) sulphate minerals [14-19]. It has been stated that the thermal decomposition of jarosite begins at 400 °C with the loss of water [1]. Water loss can occur at low temperatures over extended periods of time [1]. It is probable that in nature low temperature environments would result in the decomposition of jarosite. Recently thermogravimetric analysis has been applied to some complex mineral systems and it is considered that TG-MS analyses may also be applicable to the jarosite minerals [20-25]. The study of jarosites are important for the understanding of evaporate deposits and also for their applications in hydrometallurgy. It is important to have a fundamental understanding of the chemistry especially the thermal stability of jarosites. Such fundamental knowledge can only be obtained from thermal analysis studies. In this work we report the thermal decomposition of a synthetic ammonium jarosite using thermogravimetry and infrared emission spectroscopy.

Experimental

Minerals

An ammonium jarosite was synthesised by dissolving 1.47g of hydrated $Fe_2(SO_4)_3$ and 10.6g $(NH_4)_2SO_4$ in 75 mL of water. 5 mL of 0.375M H_2SO_4 was added to the sulfate solution in a dropwise fashion slowly over a 30 minute period. This solution was covered and heated on a hot plate at 100°C for 3 hours. A golden brown precipitate was collected under vacuum filtration and dried for 45 minutes at 100°C. The mass of dry precipitate collected was 0.56g.

X-ray diffraction

X-Ray diffraction patterns were collected using a Philips X'pert wide angle X-Ray diffractometer, operating in step scan mode, with Cu K_α radiation (1.54052 Å). Patterns were collected in the range 3 to 90° 2θ with a step size of 0.02° and a rate of 30s per step. Samples were prepared as a finely pressed powder into aluminium sample holders. The Profile Fitting option of the software uses a model that employs twelve intrinsic parameters to describe the profile, the instrumental aberration and wavelength dependent contributions to the profile.

SEM and X-ray microanalysis

Ammonium jarosite samples were coated with a thin layer of evaporated carbon and secondary electron images were obtained using an FEI Quanta 200 scanning electron microscope (SEM). For X-ray microanalysis (EDX), three samples were embedded in Araldite resin and polished with diamond paste on Lamplan 450 polishing cloth using

water as a lubricant. The samples were coated with a thin layer of evaporated carbon for conduction and examined in a JEOL 840A analytical SEM at 25kV accelerating voltage. Preliminary analyses of the samples were carried out on the FEI Quanta SEM using an EDAX microanalyser, and microanalysis of the clusters of fine crystals was carried out using a full standards quantitative procedure on the JEOL 840 SEM using a Moran Scientific microanalysis system. Oxygen was not measured directly but was calculated using assumed stoichiometries to the other elements analysed.

Thermal Analysis

Thermal decomposition of the ammonium jarosite was carried out in a TA® Instrument incorporated high-resolution thermogravimetric analyzer (series Q500) in a flowing nitrogen atmosphere (80 cm^3/min). Several analyses were undertaken; in one instance 34.4 mg of sample underwent thermal analysis, with a heating rate of 5°C/min, resolution of 6°C, to 1000°C. With the quasi-isothermal, quasi-isobaric heating program of the instrument the furnace temperature was regulated precisely to provide a uniform rate of decomposition in the main decomposition stage. The TGA instrument was coupled to a Balzers (Pfeiffer) mass spectrometer for gas analysis. Water vapour, ammonia, carbon dioxide, oxygen and sulphate as SO_2 and SO_3 were analyzed.

Raman spectroscopy

The crystals of the ammonium jarosite were placed and oriented on the stage of an Olympus BHSM microscope, equipped with 10x and 50x objectives and part of a Renishaw 1000 Raman microscope system, which also includes a monochromator, a filter system and a Charge Coupled Device (CCD). Raman spectra were excited by a HeNe laser (633 nm) at a resolution of 2 cm^{-1} in the range between 100 and 4000 cm^{-1}. Repeated acquisition using the highest magnification was accumulated to improve the signal to noise ratio. Spectra were calibrated using the 520.5 cm^{-1} line of a silicon wafer. In order to ensure that the correct spectra are obtained, the incident excitation radiation was scrambled. Previous studies by the authors provide more details of the experimental technique [26-32].

Infrared emission spectroscopy

Infrared emission spectroscopy (IES) has been applied to clay minerals [33-36]. Few applications of the technique have been used in mineral chemistry especially for the thermal decomposition of minerals [37-39]. In this paper IES is applied to the study of ammonium jarosite.

FTIR emission spectroscopy was carried out on a Nicolet infrared spectrometer, which was modified by replacing the IR source with an emission cell. A description of the cell and principles of the emission experiment have been published elsewhere. Approximately 0.2 mg of the ammonium jarosite was spread as a thin layer on a 6 mm diameter platinum surface and held in an inert atmosphere within a nitrogen-purged cell during heating. The infrared emission cell consists of a modified

atomic absorption graphite rod furnace, which is driven by a thyristor-controlled AC power supply capable of delivering up to 150 amps at 12 volts. A platinum disk acts as a hot plate to heat the jarosite sample and is placed on the graphite rod. An insulated 125-μm type R thermocouple was embedded inside the platinum plate in such a way that the thermocouple junction was <0.2 mm below the surface of the platinum. Temperature control of ± 2°C at the operating temperature of the ammonium jarosite sample was achieved by using a Eurotherm Model 808 proportional temperature controller, coupled to the thermocouple. The design of the IES facility is based on an off axis paraboloidal mirror with a focal length of 25 mm mounted above the heater capturing the infrared radiation and directing the radiation into the spectrometer. The assembly of the heating block, and platinum hot plate is located such that the surface of the platinum is slightly above the focal point of the off axis paraboloidal mirror. By this means the geometry is such that approximately 3 mm diameter area is sampled by the spectrometer. The spectrometer was modified by the removal of the source assembly and mounting a gold coated mirror, which was drilled through the centre to allow the passage of the laser beam. The mirror was mounted at 45°, which enables the IR radiation to be directed into the FTIR spectrometer.

In the normal course of events, three sets of spectra are obtained: firstly the black body radiation over the temperature range selected at the various temperatures, secondly the platinum plate radiation is obtained at the same temperatures and thirdly the spectra from the platinum plate covered with the sample. Normally only one set of black body and platinum radiation is required. The emittance spectrum at a particular temperature was calculated by subtraction of the single beam spectrum of the platinum backplate from that of the platinum + sample, and the result ratioed to the single beam spectrum of an approximate blackbody (graphite). This spectral manipulation is carried out after all the spectral data has been collected. The emission spectra were collected at intervals of 50°C over the range 200 - 750 °C. The time between scans (while the temperature was raised to the next hold point) was approximately 100 seconds. It was considered that this was sufficient time for the heating block and the powdered sample to reach temperature equilibrium. The spectra were acquired by coaddition of 64 scans for the whole temperature range (approximate scanning time 45 seconds), with a nominal resolution of 4 cm^{-1}. Good quality spectra can be obtained providing the sample thickness is not too large. If too large a sample is used then the spectra become difficult to interpret because of the presence of combination and overtone bands

In the normal course of events, three sets of spectra are obtained: first the black body radiation over the temperature range selected at the various temperatures, secondly the platinum plate radiation at the same temperatures and thirdly spectra from the platinum plate coated with the sample. Normally only one set of black body and platinum radiation data is required. The emittance spectrum (E) at a particular temperature was calculated by subtraction of the single beam spectrum of the platinum backplate from that of the platinum + sample, and the result ratioed to the single beam spectrum of an approximate blackbody (graphite). The following equation was used to calculate the emission spectra.

$$E = -0.5 * \log \frac{Pt - S}{Pt - C}$$

This manipulation is carried out after all the data is collected. Emission spectra were collected at intervals of 50°C over the range 200 - 750 °C. The time between scans (while the temperature was raised to the next hold point) was approximately 100 seconds. It was considered that this was sufficient time for the heating block and the powdered sample to reach thermal equilibrium. Spectra were acquired by 1024 scans over the temperature range 100-300°C and 128 scans over the range 350-900°C (approximate scan time 45 seconds), with a nominal resolution of 4 cm^{-1}. Good quality spectra can be obtained providing the sample thickness is not too large. If too large a sample is used then spectra become difficult to interpret because of the presence of combination and overtone bands. Spectroscopic manipulation such as baseline adjustment, smoothing and normalisation was performed using the GRAMS® software package (Galactic Industries Corporation, Salem, NH, USA).

Results and discussion

X-ray diffraction

The XRD pattern of the synthetic ammonium jarosite and the reference pattern are shown in Figure 1. The close resemblance of the two patterns shows that ammonium jarosite was synthesised. Figure 2 displays the EDX analyses of the compound equivalent to synthetic ammonium jarosite. The analysis clearly shows that the chemical composition of the compound is equivalent to ammonium jarosite. It is true that unless great lengths are taken to standardise the instrumentation EDX analyses are not reliable. Further N and O are coincidental in EDX making analyses difficult. However EDX is useful to determine the ration of Fe, S and O.

The composition of the ammonium jarosite was analysed by XPS methods. This analysis is reported in Figure 3. The analysis shows that the formula of the ammonium jarosite is $(NH_4)_{0.4}Fe_3(SO_4)_2(OH)_6$. It is not unexpected that the moles of ammonium are low. The very high vacuum of the XPS instrumentation removes volatile components such as ammonia and water. Thus the N value is low in the analysis.

Thermogravimetric Analysis and Mass spectrometric analysis

The TG and DTG graphs of ammonium jarosite $(NH_4)Fe_3(SO_4)_2\ (OH)_6$ are shown in Figure 4 and the ion current-temperature curves are shown in Figures 5a and 5b. Four mass loss steps are observed (a) from ambient to 120 °C (b) at 260 °C (c) at 389 °C (d) between 500 and 550 °C. The first mass loss is attributed to adsorbed moisture. The ion current curves (Figure 2) clearly show that water is evolved through the dehydroxylation of the mineral in two steps at 252 and 386 °C and that ammonia is evolved at 319 °C. The loss of sulphate is evidenced by the mass gain of SO_2 (M=64) as shown in Figure 3. Four distinct mass gains are observed at 394, 492, 508, 542 and 607 °C.

Using the formula of ammonium jarosite as $(NH_4)Fe_3(SO_4)_2(OH)_6$ the theoretical mass losses for ammonia, hydroxyl units as H_2O and sulphate as SO_2 are

3.54, 11.25 and 33.0 % respectively. The mass loss step at 260 °C is attributed to the dehydroxylation of the ammonium jarosite. The experimental mass loss is 15.9 % which is very different when compared with the theoretical mass loss of 11.25 %. The difference may be attributed to water trapped in the crystal structure. The experimental mass loss of ammonia is 3.3 % which corresponds well with the theoretical mass loss of 3.54 %. The experimental mass loss over the 500 to 550 ° temperature range is attributed to the loss of sulphate as SO_2. The experimental mass loss is 31.7 % compared with the theoretical mass loss of 33.0 %. The following is a suggested mechanism for the thermal decomposition of ammonium jarosite

Mechanism for the thermal decomposition of ammonium jarosite

Step 1 (up to 120 °C)

$(NH_4)Fe_3(SO_4)_2(OH)_6.xH_2O \rightarrow (NH_4)Fe_3(SO_4)_2(OH)_6 + xH_2O$

This step represents the loss of adsorbed water.

Step 2 (260 °C)

$(NH_4)Fe_3(SO_4)_2(OH)_6 \rightarrow (NH_4)(FeO)_3(SO_4)_2 + 3\ H_2O$

This step represents the dehydroxylation step with the loss of the OH units as H_2O. The ICSD database contains reference to a (NH4)Fe(SO4)2 phase, with structure related to yavapaiite, KFe(SO4)2. It is possible that this phase should be observed rather than $(NH_4)(FeO)_3(SO_4)_2$. This latter formulation should be considered as an intermediate during the decomposition. It should be noted that there was no evidence for the loss of oxygen during the experiment, even though the experiment was repeated several times. Only at elevated temperatures was the loss of oxygen observed. Drouet and Navrotsky (2003) identified the product of jarosite decomposition as yavapaiite $KFe(SO_4)_2$ [40]. On the other hand, Majzlan et al. (2004) did not identify an analogous compound in their TGA/DTA analysis of hydronium jarosite [41], so it is not quite clear whether the decomposition product is always related to yavapaiite or not.

Step 3 (389 °C)

$6(NH_4)(FeO)_3(SO_4)_2 \rightarrow 6NH_3 + 3H_2O + 3Fe_2(SO_4)_3$

This step represents the loss of ammonia and water and effectively uses up the oxygen in the formula on the LHS of the equation.

Step 4 and 5 (at 510 and 541 °C)

$2Fe_2(SO_4)_3 \rightarrow Fe_2O_3 + Fe_2(SO_4)_3 + 3SO_2$

This step represents the loss of sulphate from the iron(III) sulphate. The temperature of the decomposition is low compared with the temperature of decomposition of anhydrous iron(III) sulphate. It is noted that in the ion current curves SO_2 evolution occurs at three temperatures 508, 542 and 607 °. The first two temperatures correspond with the decomposition steps in the DTA curves. The higher temperature ion current point at 607 °C is observed in the TG curves as a broad low intensity peak at 609 °C. The mechanism of decomposition may affect the temperatures at which the sulphate decomposes. Drouet and Navrotsky found temperatures for the thermal decomposition between 550 and 700 °C. However the exact temperatures were not defined. The temperatures for the decomposition of the iron(III) sulphate are in

harmony with the values reported by Kellogg (1964) [42]. Kellogg gave the lowest temperature of decomposition as 520 °C with an average of around 640 °C. It is possible that the evolution of gases during the thermal decomposition affects the temperature for the loss of sulphate. X-ray diffraction shows that the product of the decomposition was a mixture of iron oxides.

Previous studies using TG-DTA techniques reported that the decomposition of ammonium jarosite starts at around 373 °C, with complete conversion to Fe_2O_3 at around 800 °C [13]. These authors studied the hydrothermal decomposition of ammonium jarosite by varying H_2SO_4 concentration, time, temperature and $(NH_4)_2SO_4$. The authors found that, depending on the acid molarity the jarosite was stable up to 230 °C. This value compares favourably with the value determined in this work (260 °C). At 250 °C complete decomposition of jarosite occurred within 3 hours. Other studies have determined the activation energies of the dehydration, dehydroxylation and desulphation of the ammonium jarosite [12].

Vibrational spectroscopy

One technique for studying the changes in the molecular structure is infrared emission spectroscopy. The technique enables the spectrum at the elevated temperature to be determined. In order to understand the spectrum at the elevated temperature it is necessary to understand the room temperature spectra. The Raman and infrared spectra of the ammonium jarosite are shown in Figure 6. Sulphates lend themselves to analysis by Raman spectroscopy. In aqueous systems, the sulphate anion is of T_d symmetry and is characterised by Raman bands at 981 cm^{-1} (ν_1), 451 cm^{-1}(ν_2), 1104 cm^{-1} (ν_3) and 613 cm^{-1} (ν_4). Reduction in symmetry in the crystal structure of sulphates such as jarosites will cause the splitting of these vibrational modes. For jarosites six sulphate fundamentals should be observed [43]. The Raman band at 1005 cm^{-1} is attributed to the SO_4^{2-} symmetric stretching mode. The equivalent infrared band is forbidden and is not observed.

A previous study by Sasaki reported the ammonium jarosite symmetric stretching band at 1006 cm^{-1} which is in excellent agreement with the value reported in this research [44]. The two Raman bands at 1093 and 1170 cm^{-1} are assigned to the SO_4^{2-} antisymmetric stretching modes. The two equivalent infrared bands are the two bands at 1074 and 1190 cm^{-1}. Sasaki reported the Raman bands for ammonium jarosite as 1092 and 1161 cm^{-1} in the Raman spectrum and 1080 and 1200 cm^{-1} in the infrared spectrum [44]. The band observed in the infrared spectrum at 1429 cm^{-1} is assigned to an NH bending mode.

The intense infrared band at 987 cm^{-1} is attributed to an OH librational mode. Sasaki did not report a band in this position but did show a strong band at 1000 cm^{-1}. It seems unusual to have an intense band in the infrared spectrum of the SO_4^{2-} units. The intensity of the symmetric stretching mode should approach zero for anions of this symmetry. The band at 625 cm^{-1} in the infrared spectrum and at 624 cm^{-1} in the Raman spectrum is ascribed to the ν_4 bending mode of the SO_4^{2-} units. The previous study which reported the Raman spectrum of ammonium jarosite gave two bands at 635 and 655 cm^{-1} in the infrared spectrum and at 625 cm^{-1} in the Raman spectrum

[44]. In the Raman spectrum bands at 424 and 454 cm^{-1} are attributed to the ν_2 bending modes of the SO_4^{2-} units. Two intense Raman bands are observed at 218 and 138 cm^{-1} and it is considered that these bands are related to the hydrogen of the OH units in the ammonium jarosite.

Infrared emission spectroscopy

The infrared emission spectra of the ammonium jarosite are shown in Figures 7 and 8. Figure 6 displays the OH and NH stretching region. In the 100 °C spectrum bands are resolved at 3426, 3277, 3039 and 2865 cm^{-1}. In the jarosite structure the OH and NH_4 units are equivalent. Thus the first two bands are attributed to the antisymmetric and symmetric stretching vibrations of the OH units and the latter two bands to the NH antisymmetric and symmetric stretching vibrations. The relative intensities of these bands are 15.2, 36.4, 8.5 and 2.8 %. Figure 9 shows the variation in the relative intensity of these bands as a function of temperature. The relative intensity of the 3426 and 3277 cm^{-1} bands decreases up to 300 °C. The intensity of the two bands assigned to NH stretching vibrations is reasonably constant up to 300 °C and then increases as the intensity of the OH bands approaches zero. At 450 °C no intensity remains in any of the bands.

The wavenumber region of the IES spectra between 750 and 1750 cm^{-1} are shown in Figure 9. An IR band is observed at 1003 cm^{-1} in the 100 to 200 °C spectra, the intensity of which decreases to zero in the 300 °C spectrum. This confirms the assignment of the band as an OH librational mode and not a SO_4^{2-} stretching vibration. Two bands are found at 1092 and 1075 cm^{-1} in line with the 25 °C reflectance spectrum and are attributed to the SO_4^{2-} antisymmetric stretching vibrations. The spectral definition of these bands disappears after 200 °C and is replaced by a broad band centred upon 1101 cm^{-1}. The position and intensity of this band remains constant up to 500 °C. After this temperature some definition of bands is observed. The band at 1427 cm^{-1} is observed up to 450 °C with the intensity steadily decreasing. The band is lots after the NH_4 units have been lost, confirming the assignment of the band to HNH bending vibrations.

Conclusions

Thermogravimetry combined with mass spectrometry has been used to study the thermal decomposition of a synthetic ammonium jarosite. The ammonium jarosite is stable up to 260 °C after which dehydroxylation occurs followed by de-ammoniation at 349 °C and de-sulphation by 549 °C. Changes in the molecular structure were followed using infrared emission spectroscopy.

Acknowledgments

The financial and infra-structure support of the Queensland University of Technology Inorganic Materials Research Program of the School of Physical and Chemical Sciences is gratefully acknowledged.

The Australian Research Council (ARC) is thanked for funding the thermal analysis facility.

References

1. J. E. Dutrizac and J. L. Jambor, Chapter 8 Jarosites and their application in hydrometallurgy (2000) 405.
2. E. V. Shannon, American Mineralogist 12 (1927) 424.
3. J. E. Dutrizac and J. L. Jambor, Reviews in Mineralogy & Geochemistry 40 (2000) 405.
4. K. Koiwasaki, Y. Honbou, K. Tazaki and T. Mori, Chikyu Kagaku (Chigaku Dantai Kenkyukai) 47 (1993) 493.
5. T. Buckby, S. Black, M. L. Coleman and M. E. Hodson, Mineralogical Magazine 67 (2003) 263.
6. P. A. Williams, *Oxide Zone Geochemistry*, Ellis Horwood Ltd, Chichester, West Sussex, England, 1990.
7. S. Nagai and N. Yamanouchi, Nippon Kagaku Kaishi (1921-47) 52 (1949) 83.
8. J. L. Kulp and H. H. Adler, American Journal of Science 248 (1950) 475.
9. G. Cocco, Periodico di Mineralogia 21 (1952) 103.
10. A. I. Tsvetkov and E. P. Val'yashikhina, Doklady Akademii Nauk SSSR 89 (1953) 1079.
11. A. I. Tsvetkov and E. P. Val'yashikhina, Doklady Akademii Nauk SSSR 93 (1953) 343.
12. M. Alonso, A. Lopez-Delgado and F. A. Lopez, Journal of Materials Science 33 (1998) 5821.
13. G. K. Das, S. Anand, S. Acharya and R. P. Das, Hydrometallurgy 38 (1995) 263.
14. M. S. R. Swamy, T. P. Prasad and B. R. Sant, Journal of Thermal Analysis 16 (1979) 471.
15. M. S. R. Swamy, T. P. Prasad and B. R. Sant, Journal of Thermal Analysis 15 (1979) 307.
16. S. Bhattacharyya and S. N. Bhattacharyya, Journal of Chemical and Engineering Data 24 (1979) 93.
17. M. S. R. Swami and T. P. Prasad, Journal of Thermal Analysis 19 (1980) 297.
18. M. S. R. Swamy and T. P. Prasad, Journal of Thermal Analysis 20 (1981) 107.
19. A. C. Banerjee and S. Sood, Therm. Anal., Proc. Int. Conf., 7th 1 (1982) 769.
20. R. L. Frost and K. L. Erickson, J. Therm. Anal. Calorim. 76 (2004) 217.
21. R. L. Frost, K. Erickson and M. Weier, J. Therm. Anal. Calorim. 77 (2004) 851.
22. R. L. Frost, M. L. Weier and K. L. Erickson, J. Therm. Anal. Calorim. 76 (2004) 1025.
23. R. L. Frost and M. L. Weier, J. Therm. Anal. Calorim. 75 (2004) 277.
24. R. L. Frost, W. Martens, Z. Ding and J. T. Kloprogge, J. Therm. Anal. Calorim. 71 (2003) 429.
25. R. L. Frost, Z. Ding and H. D. Ruan, J. Therm. Anal. Calorim. 71 (2003) 783.
26. R. L. Frost, J. Raman Spectrosc. 35 (2004) 153.
27. R. L. Frost, Spectrochim. Acta, Part A 60A (2004) 1439.
28. R. L. Frost, O. Carmody, K. L. Erickson, M. L. Weier, D. O. Henry and J. Cejka, J. Mol. Struct. 733 (2004) 203.
29. R. L. Frost, L. Duong and M. Weier, Spectrochim. Acta, Part A 60 (2004) 1853.
30. R. L. Frost and M. Weier, Neues Jahrb. Mineral., Monatsh. (2004) 445.
31. R. L. Frost and M. L. Weier, J. Raman Spectrosc. 35 (2004) 299.

32. R. L. Frost, M. L. Weier and M. O. Adebajo, Thermochim. Acta 419 (2004) 119.
33. R. L. Frost, P. M. Fredericks, B. M. Collins, A. J. Vassallo and K. A. Finnie, in *10th International Clay Conference* (Eds.: W. Fitzpatrick, G. J. ChurchmanandT. Eggleton), Adelaide, Australia, 1994.
34. R. L. Frost and A. M. Vassallo, Clays Clay Miner. 44 (1996) 635.
35. R. L. Frost and S. M. Dutt, J. Colloid Interface Sci. 198 (1998) 330.
36. R. L. Frost and J. T. Kloprogge, Spectrochim. Acta, Part A 55A (1999) 2195.
37. R. L. Frost, Z. Ding, J. T. Kloprogge and W. N. Martens, Thermochim. Acta 390 (2002) 133.
38. R. L. Frost, M. L. Weier, W. Martens, J. T. Kloprogge and Z. Ding, Thermochim. Acta 401 (2003) 121.
39. R. L. Frost and M. L. Weier, Thermochim. Acta 406 (2003) 221.
40. C. Drouet and A. Navrotsky, Geochimica et Cosmochimica Acta 67 (2003) 2063.
41. J. Majzlan, R. Stevens, J. Boerio-Goates, B. F. Woodfield, A. Navrotsky, P. C. Burns, M. K. Crawford and T. G. Amos, Physics and Chemistry of Minerals 31 (2004) 518.
42. H. H. Kellogg, Transactions of the American Institute of Mining, Metallurgical and Petroleum Engineers 230 (1964) 1622.
43. V. C. Farmer, *Mineralogical Society Monograph 4: The Infrared Spectra of Minerals*, 1974.
44. K. Sasaki, O. Tanaike and H. Konno, Canadian Mineralogist 36 (1998) 1225.

List of Figures

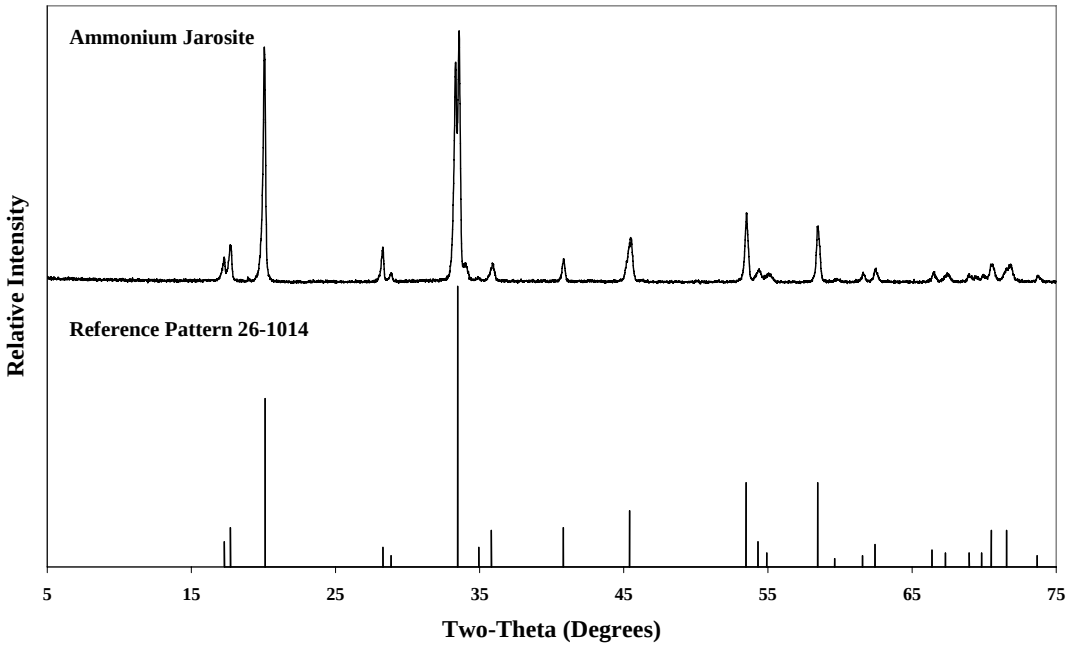

Figure 1

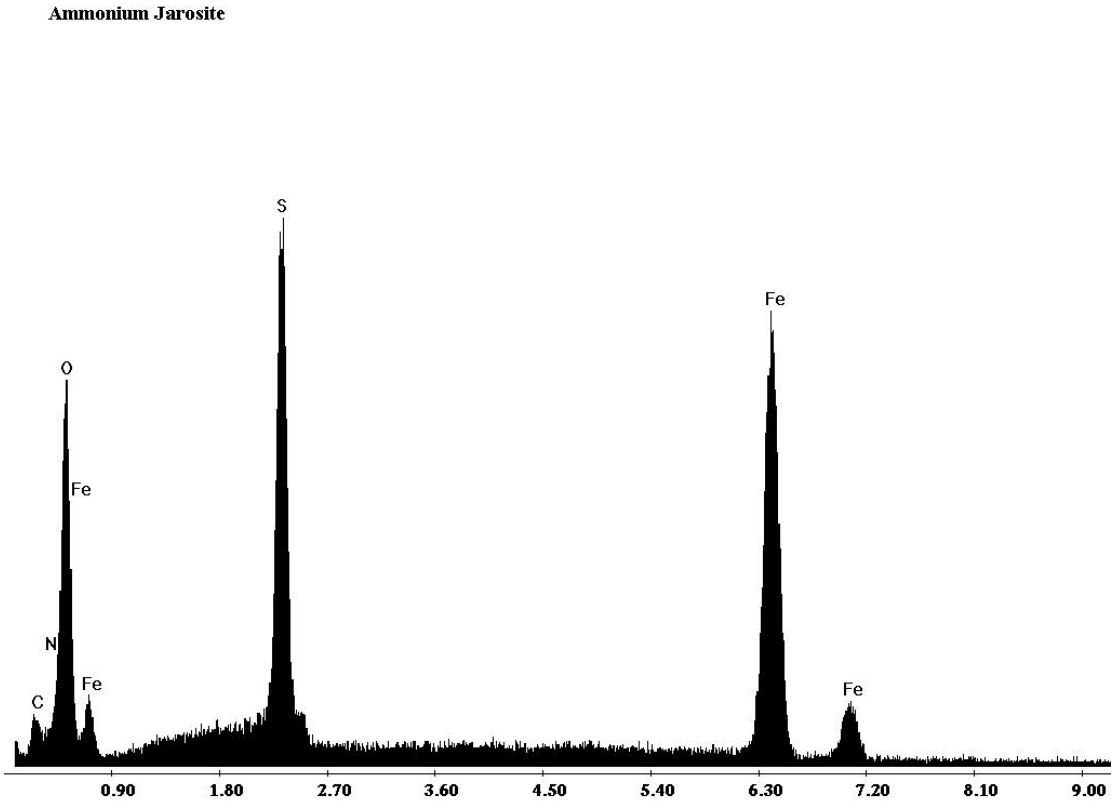

Figure 2

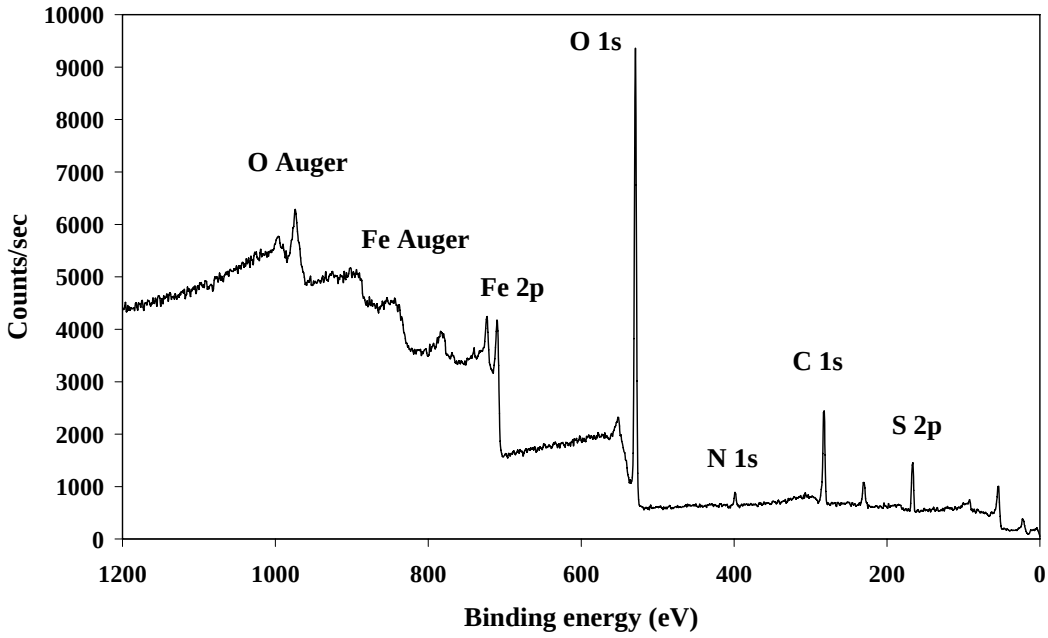
10000
9000
8000
7000
6000
5000
4000
3000
2000
1000
0
Counts/sec
O 1s
O Auger
Fe Auger
Fe 2p
C 1s
S 2p
N 1s
1200
1000
800
600
400
200
0
Binding energy (eV)

Figure 3

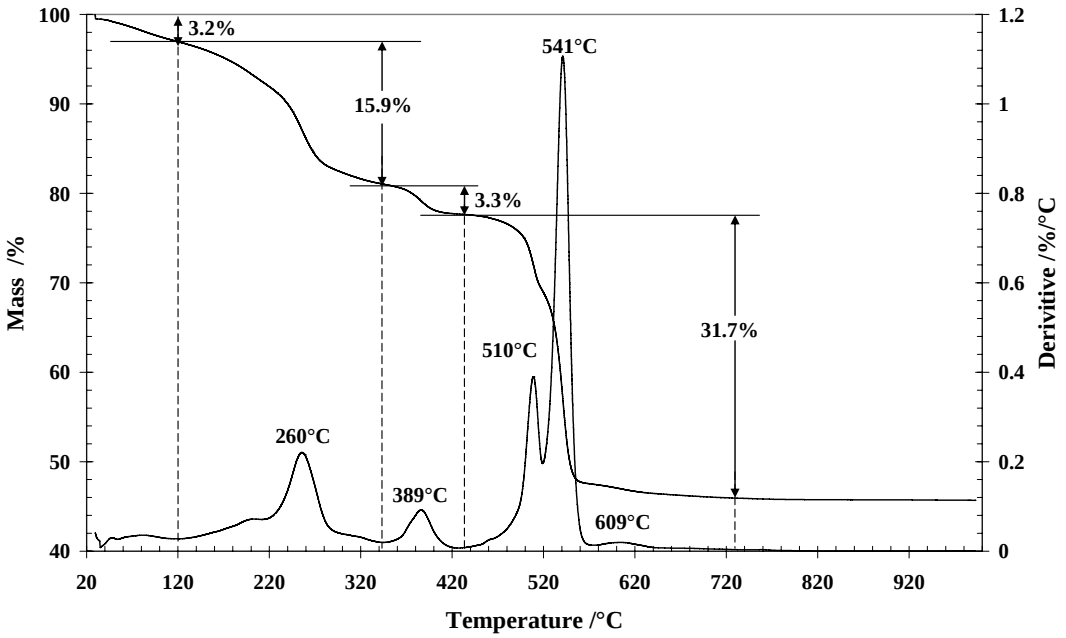
100
90
80
70
60
50
40
Mass /%
1.2
1
0.8
0.6
0.4
0.2
0
Derivitive /%/°C
20
120
220
320
420
520
620
720
820
920
Temperature /°C
3.2%
15.9%
3.3%
31.7%
541°C
510°C
260°C
389°C
609°C

Figure 4

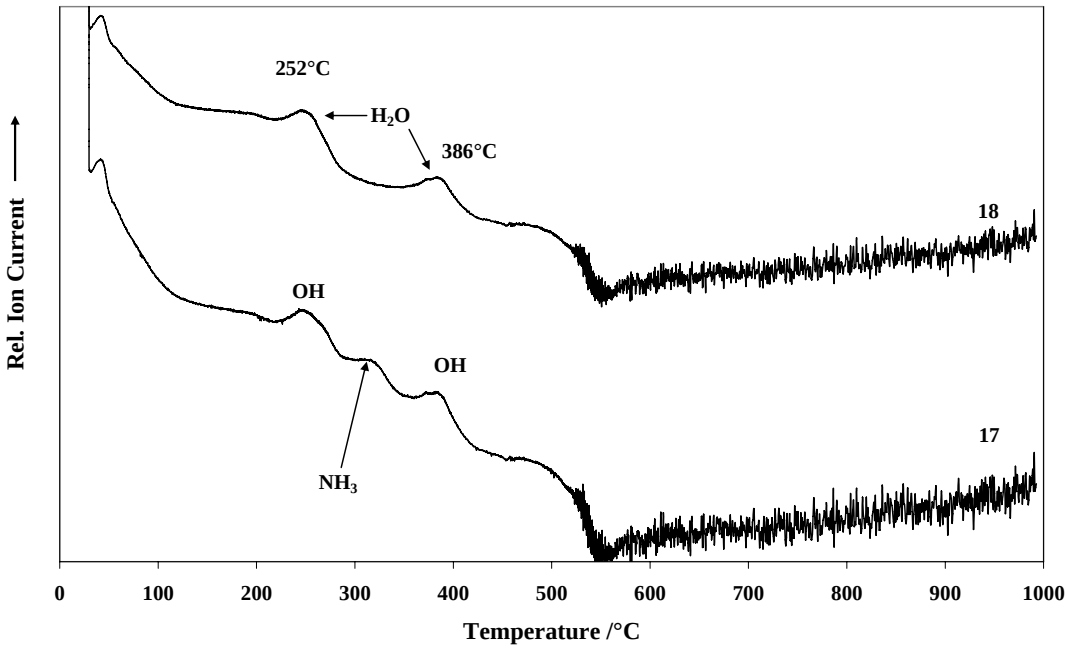

Figure 5a

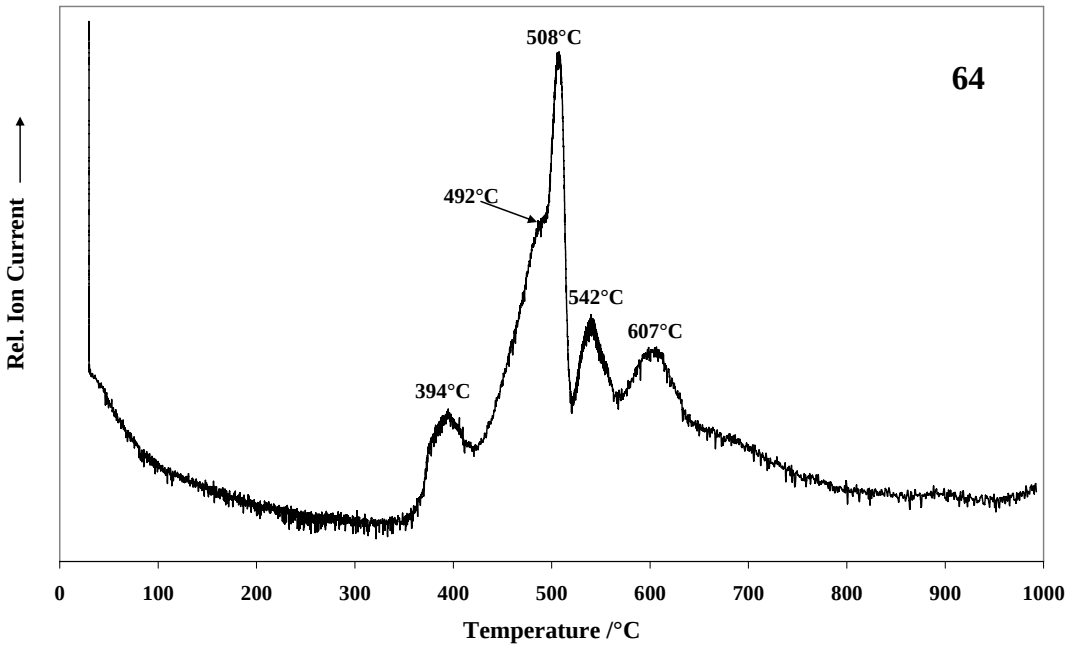

Figure 5b

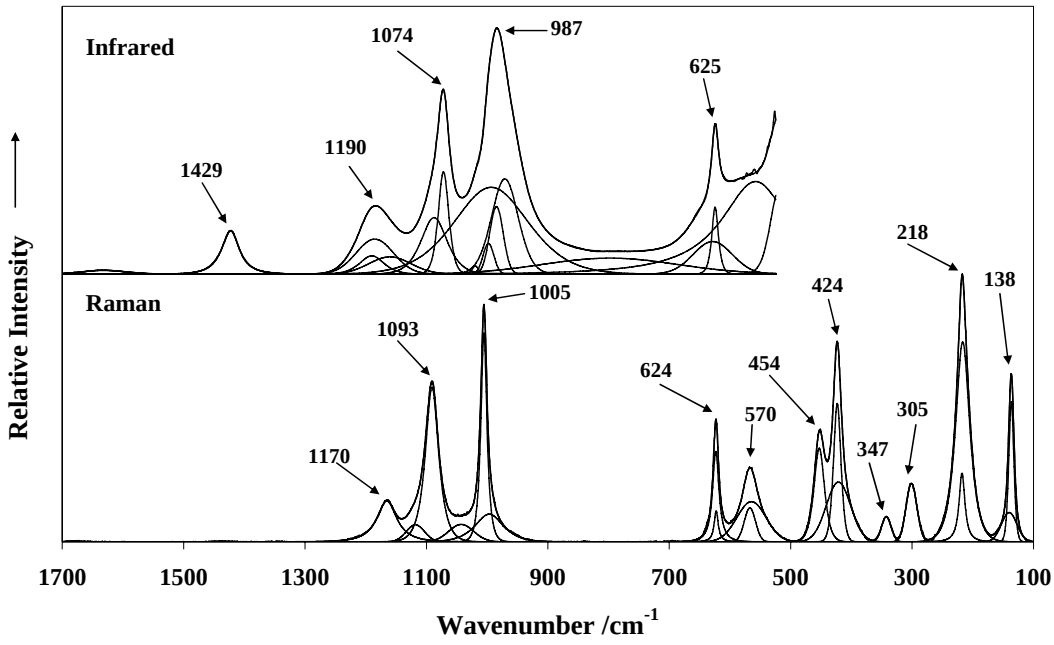
Infrared
1074
987
625
1190
1429
Raman
1005
1093
624
454
424
218
138
570
305
347
1170
Relative Intensity
1700
1500
1300
1100
900
700
500
300
100
Wavenumber /cm-1

Figure 6

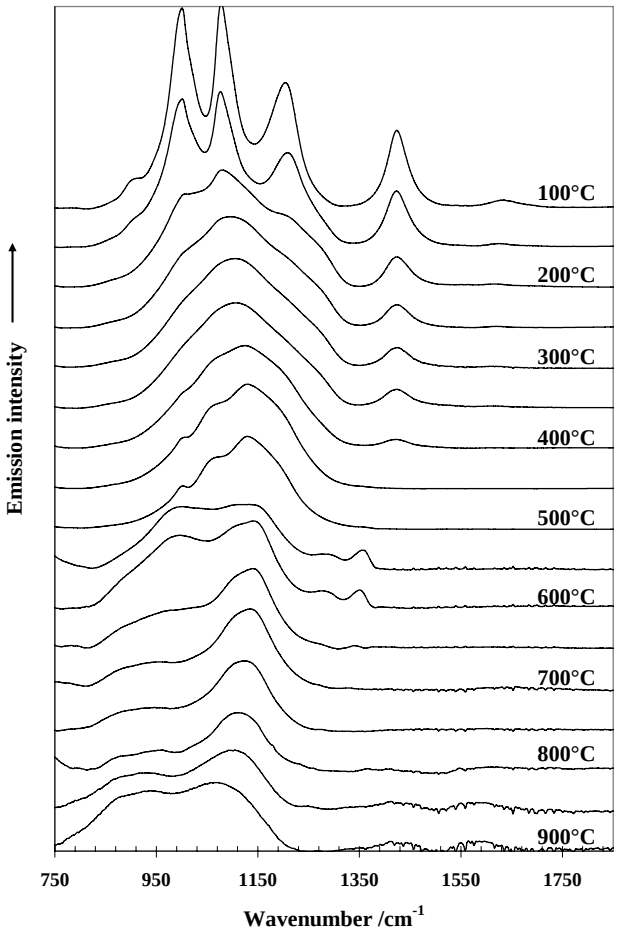
Emission intensity
100°C
200°C
300°C
400°C
500°C
600°C
700°C
800°C
900°C
750
950
1150
1350
1550
1750
Wavenumber /cm-1

Figure 7

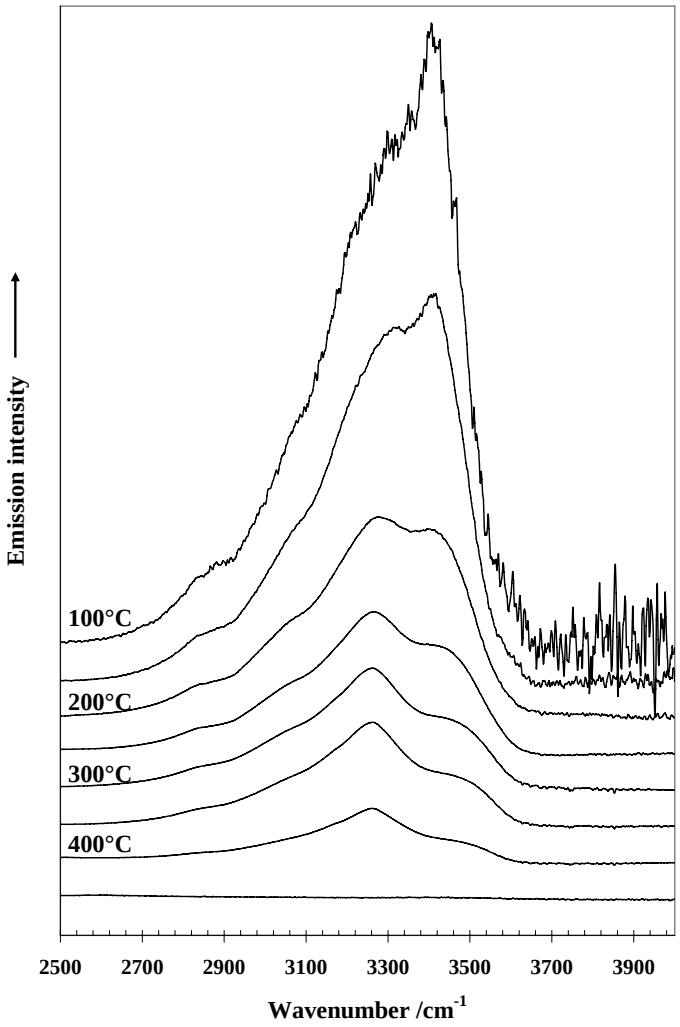
Emission intensity
100°C
200°C
300°C
400°C
2500
2700
2900
3100
3300
3500
3700
3900
Wavenumber /cm-1

Figure 8

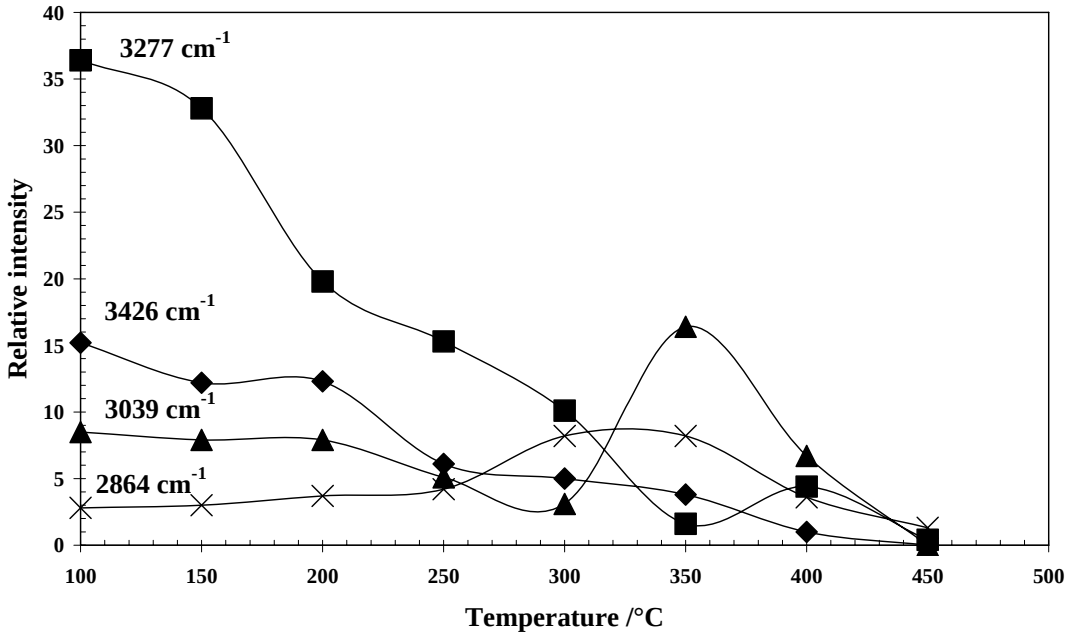
3277 cm-1
3426 cm-1
3039 cm-1
2864 cm-1
Relative intensity
Temperature /°C
0
5
10
15
20
25
30
35
40
100
150
200
250
300
350
400
450
500

Figure 9